A meshless algorithm with moving least square approximations for elliptic Signorini problems*

Wang Yan-Chong(王延冲) and Li Xiao-Lin(李小林)†

College of Mathematics Science, Chongqing Normal University, Chongqing 400047, *China*

(Received 2 December 2013; revised manuscript received 13 March 2014; published online 9 July 2014)

Based on the moving least square (MLS) approximations and the boundary integral equations (BIEs), a meshless algorithm is presented in this paper for elliptic Signorini problems. In the algorithm, a projection operator is used to tackle the nonlinear boundary inequality conditions. The Signorini problem is then reformulated as BIEs and the unknown boundary variables are approximated by the MLS approximations. Accordingly, only a nodal data structure on the boundary of a domain is required. The convergence of the algorithm is proven. Numerical examples are given to show the high convergence rate and high computational efficiency of the presented algorithm.

Keywords: meshless method, Signorini problem, moving least square approximations, convergence

PACS: 02.60.Cb, 02.60.Lj, 02.30.Em **DOI:** 10.1088/1674-1056/23/9/090202

1. Introduction

In 1933, Signorini[1] studied a problem in elasticity with contact boundary conditions from which the term the Signorini problem was coined. In 1964, Fichera[2] gave the proof of the existence and the regularity of a weak solution, and discussed the uniqueness of the solution. Signorini problems involve the determination of an unknown free boundary and are important to many branches of engineering and science. Many physical phenomena, such as the fluid mechanics problems in media with semipermeable boundaries, the elasticity with contact conditions, the free boundary problems, the dam problem, and the electropainting problem, can be described as Signorini problems.[3–5]

In the past three decades, the finite difference method,[6] the finite element method (FEM),[3,4] and the boundary element method (BEM)[7–11] for the Signorini problems have been developed. The success of those methods depends critically on the ability to generate and maintain meshes of sufficient quality throughout the whole simulation. The mesh generation in some situations is time consuming, arduous, and fraught with pitfalls.

In recent years, meshless (or meshfree) methods have attached much attention for solving boundary value problems. This type of method alleviates the difficulty of meshing and remeshing the entire structure by simply adding or deleting nodes. Meshless methods have developed so fast that they are applied successfully to a variety of science and engineering problems.

The moving least square (MLS)[12] is an approximation scheme of constructing continuous functions from a set of unorganized sampled point values. Recently, some MLS variants have also been presented.[13–17] Since the numerical approximations start from scattered nodes instead of elements, the MLS scheme is one of the most extensively used schemes to form the meshless shape functions. Some MLS-based meshless methods, such as the element-free Galerkin method, the h–p meshless method, and the meshless local Petrov–Galerkin method have been developed and achieved remarkable success in solving a broad range of physical problems.[18–21] They are the domain type, as the FEM, in which the problem domain is discretized by nodes.

The boundary integral equation (BIE) is an important and attractive computational tool as it can reduce the dimensionality of the considered problem by one. The meshless boundary integral equation method is an important direction of the meshless method. Combining the MLS scheme with BIEs, some meshless boundary integral equation methods have been developed, such as the boundary node method (BNM),[22] the hybrid BNM,[23–25] the boundary element-free method,[26–28] and the symmetrical Galerkin BNM.[29–31] Compared with the domain type meshless methods, they require only a nodal data structure on the bounding surface of a body whose dimension is less than that of the domain itself. Therefore, they have emerged as promising numerical techniques in scientific computing.

In this paper, based on the MLS approximation, a meshless boundary integral equation algorithm is developed for elliptic Signorini problems. The algorithm only requires nodes generated on the boundary of the domain. In Signorini problems, the Signorini boundary conditions are in the form of nonlinear inequalities involving the unknown function and its derivative together with a complementarity relation. In this

*Project supported by the National Natural Science Foundation of China (Grant No. 11101454), the Natural Science Foundation of Chongqing CSTC, China (Grant No. cstc2014jcyjA00005), and the Program of Innovation Team Project in University of Chongqing City, China (Grant No. KJTD201308).

†Corresponding author. E-mail: lxlmath@163.com

© 2014 Chinese Physical Society and IOP Publishing Ltd

algorithm, these nonlinear conditions are incorporated into an iterative scheme and thus can be applied with ease. As the nonlinear inequality conditions lie on the boundary of the domain and the boundary is of prime interest, the present algorithm is suitable for Signorini problems. The convergence of this algorithm is also derived theoretically. The numerical examples show that this meshless algorithm is very effective, and has good convergent character and computational efficiency.

The rest of this paper is organized as follows. In Section 2, BIEs for Signorini problems are described. In Section 3, boundary variable approximations are provided. Then, a detailed numerical implementation for Signorini problems is provided in Section 4. In Section 5, a convergence study of this meshless algorithm is presented. In Section 6, some numerical examples are given. Finally, the conclusions are drawn from the present study.

2. Signorini problems and BIEs

Let Ω be a domain bounded by Γ, which is divided into three nonoverlapping parts: the Dirichlet boundary $\Gamma_{\rm D}$, Neumann boundary $\Gamma_{\rm N}$, and Signorini boundary $\Gamma_{\rm S}$, such that $\Gamma=\Gamma_{\rm D}\cup\Gamma_{\rm N}\cup\Gamma_{\rm S}$ and $\Gamma_{\rm S}\neq\emptyset$. The governing equation for the Signorini problems can be written as

$$\mathcal{L}u(\boldsymbol{x})=b(\boldsymbol{x}),\qquad \boldsymbol{x}\in\Omega, \tag{1}$$

with the Dirichlet and the Neumann boundary conditions

$$u(\boldsymbol{x})=\bar{u}(\boldsymbol{x}),\qquad \boldsymbol{x}\in\Gamma_{\rm D}, \tag{2}$$

$$q(\boldsymbol{x})=\bar{q}(\boldsymbol{x}),\qquad \boldsymbol{x}\in\Gamma_{\rm N}, \tag{3}$$

and the Signorini boundary conditions

$$\begin{aligned}&u(\boldsymbol{x})\le\bar{u}(\boldsymbol{x}),\qquad q(\boldsymbol{x})\le\bar{q}(\boldsymbol{x}),\\&(u(\boldsymbol{x})-\bar{u}(\boldsymbol{x}))(q(\boldsymbol{x})-\bar{q}(\boldsymbol{x}))=0,\qquad \boldsymbol{x}\in\Gamma_{\rm S},\end{aligned} \tag{4}$$

where $\mathcal{L}$ is a uniformly elliptic and self-adjoint second order partial differential operator without loss of generality, $u(\boldsymbol{x})$ is an unknown function, $q(\boldsymbol{x})$ is the conformal derivative of $u(\boldsymbol{x})$ on Γ, $b(\boldsymbol{x})$ is a known function, and $\bar{u}(\boldsymbol{x})$ and $\bar{q}(\boldsymbol{x})$ are the prescribed boundary functions.

In Signorini problems, we need to determine the part of $\Gamma_{\rm S}$ on which conditions $u=\bar{u}$ and $q<\bar{q}$ apply and the remaining part on which conditions $u<\bar{u}$ and $q=\bar{q}$ apply.

To tackle the nonlinear Signorini boundary conditions (4), we define an operator[6,7,11,32]

$$[v]_-=\min(v,0),\qquad v\in\mathbb{R}.$$

Then, conditions (4) may equivalently be formulated as

$$\begin{aligned}u(\boldsymbol{x})-\bar{u}(\boldsymbol{x})=&[(u(\boldsymbol{x})-\bar{u}(\boldsymbol{x}))-c(q(\boldsymbol{x})-\bar{q}(\boldsymbol{x}))]_-,\\&\boldsymbol{x}\in\Gamma_{\rm S},\end{aligned} \tag{5}$$

where c is an arbitrary but fixed positive constant. Thus, we define an iterative scheme on $\Gamma_{\rm S}$ as

$$\begin{aligned}u^{(k+1)}(\boldsymbol{x})=\bar{u}(\boldsymbol{x})+&\left[(u^{(k)}(\boldsymbol{x})-\bar{u}(\boldsymbol{x}))-c(q^{(k+1)}(\boldsymbol{x})-\bar{q}(\boldsymbol{x}))\right]_-,\\&k=0,1,2,\ldots,\ \boldsymbol{x}\in\Gamma_{\rm S}.\end{aligned} \tag{6}$$

To implement Eq. (6) numerically, the boundary conditions on $\Gamma_{\rm S}$ need to be verified point-wise. If on some parts of $\Gamma_{\rm S}$, denoted as $\Gamma_{\rm SD}$, inequality

$$\left(u^{(k)}(\boldsymbol{x})-\bar{u}(\boldsymbol{x})\right)-c\left(q^{(k)}(\boldsymbol{x})-\bar{q}(\boldsymbol{x})\right)>0$$

is true, then the boundary condition is imposed as

$$u^{(k+1)}(\boldsymbol{x})=\bar{u}(\boldsymbol{x}),\qquad \boldsymbol{x}\in\Gamma_{\rm SD} \tag{7}$$

for the next iteration. On the remaining parts of $\Gamma_{\rm S}$, denoted as $\Gamma_{\rm SR}$, the boundary condition is imposed as

$$u^{(k+1)}(\boldsymbol{x})=u^{(k)}(\boldsymbol{x})-c\left(q^{(k+1)}(\boldsymbol{x})-\bar{q}(\boldsymbol{x})\right),\quad \boldsymbol{x}\in\Gamma_{\rm SR}. \tag{8}$$

Consequently, the original Signorini problem (1)–(4) is converted into a sequence of well-posed problems

$$\begin{cases}\mathcal{L}u^{(k+1)}(\boldsymbol{x})=b(\boldsymbol{x}), & \boldsymbol{x}\in\Omega,\\ u^{(k+1)}(\boldsymbol{x})=\bar{u}(\boldsymbol{x}), & \boldsymbol{x}\in\Gamma_{\rm D}\cup\Gamma_{\rm SD},\\ q^{(k+1)}(\boldsymbol{x})=\bar{q}(\boldsymbol{x}), & \boldsymbol{x}\in\Gamma_{\rm N},\\ u^{(k+1)}(\boldsymbol{x})=u^{(k)}(\boldsymbol{x})-c\left(q^{(k+1)}(\boldsymbol{x})-\bar{q}(\boldsymbol{x})\right), & \boldsymbol{x}\in\Gamma_{\rm SR}.\end{cases} \tag{9}$$

In the following, problem (9) is solved by a meshless boundary integral equation method to obtain $u^{(k+1)}$ and $q^{(k+1)}$ on $\Gamma_{\rm S}$.

The BIE for the solution of problem (9) is[33]

$$\begin{aligned}C(\boldsymbol{y})u^{(k+1)}(\boldsymbol{y})=&\int_\Gamma u^*(\boldsymbol{x},\boldsymbol{y})q^{(k+1)}(\boldsymbol{x})\,{\rm d}\Gamma\\&-\int_\Gamma q^*(\boldsymbol{x},\boldsymbol{y})u^{(k+1)}(\boldsymbol{x})\,{\rm d}\Gamma\\&-\int_\Omega u^*(\boldsymbol{x},\boldsymbol{y})b(\boldsymbol{x})\,{\rm d}\Omega,\qquad \boldsymbol{y}\in\Gamma,\end{aligned} \tag{10}$$

where $\boldsymbol{x}$ is the field point, $\boldsymbol{y}$ is the source point located on boundary Γ, $C(\boldsymbol{y})$ is the function of the internal angle that boundary Γ makes at the given point $\boldsymbol{y}$, $u^*(\boldsymbol{x},\boldsymbol{y})$ is the fundamental solution of the differential operator $\mathcal{L}$, and $q^*(\boldsymbol{x},\boldsymbol{y})$ is the conformal derivative of $u^*(\boldsymbol{x},\boldsymbol{y})$ with respect to $\boldsymbol{x}$ on Γ.

3. Boundary variable approximation

Let $\{\boldsymbol{y}_i\}_{i=1}^N$ be a set of N boundary nodes $\boldsymbol{y}_i\in\Gamma$. We approximate $u^{(k+1)}$ and $q^{(k+1)}$ at the boundary Γ by the MLS approximation as[29,30]

$$u^{(k+1)}(\boldsymbol{x})=\sum_{i=1}^N\Phi_i(\boldsymbol{x})\hat{u}_i^{(k+1)}, \tag{11}$$

$$q^{(k+1)}(\boldsymbol{x})=\sum_{i=1}^N\Phi_i(\boldsymbol{x})\hat{q}_i^{(k+1)}, \tag{12}$$

where $\hat{u}_i^{(k+1)}=\hat{u}^{(k+1)}(\boldsymbol{y}_i)$ and $\hat{q}_i^{(k+1)}=\hat{q}^{(k+1)}(\boldsymbol{y}_i)$ are the nodal values. $\Phi_i(\boldsymbol{x})$ is the shape function of the MLS approximation corresponding to node $\boldsymbol{y}_i$, which is given by

$$\Phi_i(\boldsymbol{x}) = \begin{cases} \sum_{j=0}^{m} P_j(\boldsymbol{s}) \left[\boldsymbol{A}^{-1}(\boldsymbol{s}) \boldsymbol{B}(\boldsymbol{s})\right]_{jk}, & i = I_k \in \wedge(\boldsymbol{x}), \\ 0, & i \notin \wedge(\boldsymbol{x}), \end{cases} \quad 1 \le i \le N,$$

where $\boldsymbol{s}$ is a local coordinate of the boundary point $\boldsymbol{x}$ on Γ, $P_j(\boldsymbol{s})$ is a basis of order m consisting of monomials in $\boldsymbol{s}$, $\wedge(\boldsymbol{x}) = \{I_1, I_2, \ldots, I_\kappa\}$ is the set of the global sequence numbers of the boundary nodes that lie on the influence domain of $\boldsymbol{x}$, and the matrices $\boldsymbol{A}(\boldsymbol{s})$ and $\boldsymbol{B}(\boldsymbol{s})$ are defined as

$$\boldsymbol{A}(\boldsymbol{s}) = \sum_{j \in \wedge(\boldsymbol{x})} w_j(\boldsymbol{s}) \boldsymbol{P}(\boldsymbol{s}_j) \boldsymbol{P}^{\mathrm{T}}(\boldsymbol{s}_j),$$

$$\boldsymbol{B}(\boldsymbol{s}) = \left[w_{I_1}(\boldsymbol{s}) \boldsymbol{P}(\boldsymbol{s}_{I_1}), w_{I_2}(\boldsymbol{s}) \boldsymbol{P}(\boldsymbol{s}_{I_2}), \cdots, w_{I_\kappa}(\boldsymbol{s}) \boldsymbol{P}(\boldsymbol{s}_{I_\kappa})\right],$$

in which $w_j(\boldsymbol{s})$ is a weight function and $\boldsymbol{s}_j$ is the curvilinear co-ordinate of node $\boldsymbol{y}_j$.

4. Discretization and numerical implementation

Substituting Eqs. (11) and (12) into Eq. (10) for boundary node $\boldsymbol{y}_j$ yields

$$\begin{aligned} & C(\boldsymbol{y}_j) \sum_{i=1}^{N} \Phi_i(\boldsymbol{y}_j) \hat{u}_i^{(k+1)} \\ &= \int_\Gamma u^*(\boldsymbol{x}, \boldsymbol{y}_j) \sum_{i=1}^{N} \Phi_i(\boldsymbol{x}) \hat{q}_i^{(k+1)} \mathrm{d}\Gamma \\ &\quad - \int_\Gamma q^*(\boldsymbol{x}, \boldsymbol{y}_j) \sum_{i=1}^{N} \Phi_i(\boldsymbol{x}) \hat{u}_i^{(k+1)} \mathrm{d}\Gamma - \int_\Omega u^*(\boldsymbol{x}, \boldsymbol{y}_j) b(\boldsymbol{x}) \mathrm{d}\Omega. \end{aligned} \tag{13}$$

To carry out numerical integration, the boundary Γ is separated into nonoverlapping integration sub-domains Γ_I ($I = 1, 2, \ldots, N_\Gamma$) such that $\Gamma = \bigcup_{I=1}^{N_\Gamma} \Gamma_I$. Here, N_Γ is the total number of the sub-domains. It is stressed that Γ_I is not a boundary element, so no shape function is dependent on it. In this paper, these sub-domains are only used so that the integrals in Eq. (13) can be obtained numerically. Equation (13) can then be written as

$$\begin{aligned} & C(\boldsymbol{y}_j) \sum_{i=1}^{N} \Phi_i(\boldsymbol{y}_j) \hat{u}_i^{(k+1)} \\ &= \sum_{i=1}^{N} \hat{q}_i^{(k+1)} \sum_{I=1}^{N_\Gamma} \int_{\Gamma_I} u^*(\boldsymbol{x}, \boldsymbol{y}_j) \Phi_i(\boldsymbol{x}) \mathrm{d}\Gamma \\ &\quad - \sum_{i=1}^{N} \hat{u}_i^{(k+1)} \sum_{I=1}^{N_\Gamma} \int_{\Gamma_I} q^*(\boldsymbol{x}, \boldsymbol{y}_j) \Phi_i(\boldsymbol{x}) \mathrm{d}\Gamma - \sum_{e=1}^{N_e} \left[\sum_{I=1}^{N_I} w_I (u^* b)_I\right] A_e, \end{aligned} \tag{14}$$

where w_I is the integration weight, the function $u^* b$ needs to be evaluated at the I integration points, N_I is the total number of integration points, N_e is the number of cells into which Ω has been divided, and A_e is the area of each cell.

Using Eq. (14) for all nodes $\boldsymbol{y}_j$ and applying the numerical scheme for integrals, we have the following linear algebraic equation:

$$\boldsymbol{H}\hat{\boldsymbol{U}} + \boldsymbol{G}\hat{\boldsymbol{Q}} = \bar{\boldsymbol{B}}, \tag{15}$$

where

$$\hat{\boldsymbol{U}} = \left(\hat{u}_1^{(k+1)}, \hat{u}_2^{(k+1)}, \ldots, \hat{u}_N^{(k+1)}\right)^{\mathrm{T}},$$

$$\hat{\boldsymbol{Q}} = \left(\hat{q}_1^{(k+1)}, \hat{q}_2^{(k+1)}, \ldots, \hat{q}_N^{(k+1)}\right)^{\mathrm{T}},$$

$\boldsymbol{H}$ and $\boldsymbol{G}$ are the corresponding coefficient matrices, and $\bar{\boldsymbol{B}} = (\bar{B}_1, \bar{B}_2, \ldots, \bar{B}_N)^{\mathrm{T}}$ with $\bar{B}_i = -\sum_{e=1}^{N_e} \left[\sum_{I=1}^{N_I} w_I (u^* b)_I\right] A_e$.

In order to determine the unknown $\hat{\boldsymbol{U}}$ and $\hat{\boldsymbol{Q}}$, the boundary conditions must be imposed. For the convenience of discussion, we assume that the first N_d boundary nodes $\{\boldsymbol{y}_j\}_{j=1}^{N_\mathrm{d}} \subset \Gamma_\mathrm{D} \cup \Gamma_\mathrm{SD}$, the next N_n boundary nodes $\{\boldsymbol{y}_j\}_{j=N_\mathrm{d}+1}^{N_\mathrm{d}+N_\mathrm{n}} \subset \Gamma_\mathrm{N}$, and the rest $N_\mathrm{r} = N - N_\mathrm{d} - N_\mathrm{n}$ boundary nodes $\{\boldsymbol{y}_j\}_{j=N_\mathrm{d}+N_\mathrm{n}+1}^{N} \subset \Gamma_\mathrm{SR}$.

Using Eq. (11) for all nodes $\{\boldsymbol{y}_j\}_{j=1}^{N_\mathrm{d}} \subset \Gamma_\mathrm{D} \cup \Gamma_\mathrm{SD}$ yields

$$u^{(k+1)}(\boldsymbol{y}_j) = \sum_{i=1}^{N} \Phi_i(\boldsymbol{y}_j) \hat{u}_i^{(k+1)},$$

which can be expressed as

$$\boldsymbol{M}_1 \hat{\boldsymbol{U}} = \bar{\boldsymbol{U}}_1, \tag{16}$$

where $\bar{\boldsymbol{U}}_1 = \left(\bar{u}^{(k+1)}(\boldsymbol{y}_1), \bar{u}^{(k+1)}(\boldsymbol{y}_2), \ldots, \bar{u}^{(k+1)}(\boldsymbol{y}_{N_\mathrm{d}})\right)^{\mathrm{T}}$ is given by the boundary conditions on $\Gamma_\mathrm{D} \cup \Gamma_\mathrm{SD}$.

Besides, using Eq. (12) for all nodes $\{\boldsymbol{y}_j\}_{j=N_\mathrm{d}+1}^{N_\mathrm{d}+N_\mathrm{n}} \subset \Gamma_\mathrm{N}$ yields

$$q^{(k+1)}(\boldsymbol{y}_j) = \sum_{i=1}^{N} \Phi_i(\boldsymbol{y}_j) \hat{q}_i^{(k+1)},$$

which can be expressed as

$$\boldsymbol{M}_2 \hat{\boldsymbol{Q}} = \bar{\boldsymbol{Q}}_2, \tag{17}$$

where

$$\bar{\boldsymbol{Q}}_2 = \left(\bar{q}^{(k+1)}(\boldsymbol{y}_{N_\mathrm{d}+1}), \bar{q}^{(k+1)}(\boldsymbol{y}_{N_\mathrm{d}+2}), \ldots, \bar{q}^{(k+1)}(\boldsymbol{y}_{N_\mathrm{d}+N_\mathrm{n}})\right)^{\mathrm{T}}$$

is given by the boundary conditions on Γ_N.

Moreover, using Eqs. (11) and (12) for all nodes $\{\boldsymbol{y}_j\}_{j=N_\mathrm{d}+N_\mathrm{n}+1}^{N} \subset \Gamma_\mathrm{SR}$ yields

$$\boldsymbol{M}_3 \hat{\boldsymbol{U}} = \boldsymbol{U}_3, \tag{18}$$

$$\boldsymbol{M}_3 \hat{\boldsymbol{Q}} = \boldsymbol{Q}_3, \tag{19}$$

where $\boldsymbol{U}_3 = \left(u^{(k+1)}(\boldsymbol{y}_{N_\mathrm{d}+N_\mathrm{n}+1}), \ldots, u^{(k+1)}(\boldsymbol{y}_N)\right)^{\mathrm{T}}$ and $\boldsymbol{Q}_3 = \left(q^{(k+1)}(\boldsymbol{y}_{N_\mathrm{d}+N_\mathrm{n}+1}), \ldots, q^{(k+1)}(\boldsymbol{y}_N)\right)^{\mathrm{T}}$ are unknowns at the nodes on boundary Γ_SR.

Furthermore, collocating the Robin boundary conditions (8) at nodes $\{\boldsymbol{y}_j\}_{j=N_\mathrm{d}+N_\mathrm{n}+1}^{N} \subset \Gamma_\mathrm{SR}$ yields

$$u^{(k+1)}(\boldsymbol{y}_j) = u^{(k)}(\boldsymbol{y}_j) - c\left(q^{(k+1)}(\boldsymbol{y}_j) - \bar{q}(\boldsymbol{y}_j)\right),$$

which can be expressed as

$$\boldsymbol{U}_3 = \bar{\boldsymbol{F}} - c\boldsymbol{Q}_3, \tag{20}$$

where $\bar{\boldsymbol{F}} = \left(f_{N_\mathrm{d}+N_\mathrm{n}+1}, f_{N_\mathrm{d}+N_\mathrm{n}+2}, \ldots, f_N\right)^\mathrm{T}$ is given with $f_j = u^{(k)}(\boldsymbol{y}_j) + c\bar{q}(\boldsymbol{y}_j)$. Inserting Eqs. (18) and (19) into Eq. (20) leads to

$$\boldsymbol{M}_3\hat{\boldsymbol{U}} + c\boldsymbol{M}_3\hat{\boldsymbol{Q}} = \bar{\boldsymbol{F}}. \tag{21}$$

Gathering Eqs. (15)–(17) and (21) leads to the following linear algebraic equation:

$$\begin{bmatrix} \boldsymbol{H} & \boldsymbol{G} \\ \boldsymbol{M}_1 & \boldsymbol{0} \\ \boldsymbol{0} & \boldsymbol{M}_2 \\ \boldsymbol{M}_3 & c\boldsymbol{M}_3 \end{bmatrix} \begin{bmatrix} \hat{\boldsymbol{U}} \\ \hat{\boldsymbol{Q}} \end{bmatrix} = \begin{bmatrix} \bar{\boldsymbol{B}} \\ \bar{\boldsymbol{U}}_1 \\ \bar{\boldsymbol{Q}}_2 \\ \bar{\boldsymbol{F}} \end{bmatrix}. \tag{22}$$

Equation (22) is now first solved for the unknown $\hat{\boldsymbol{U}}$ and $\hat{\boldsymbol{Q}}$, then the unknown $u^{(k+1)}(\boldsymbol{y}_j)$ and $q^{(k+1)}(\boldsymbol{y}_j)$ for all nodes $\boldsymbol{y}_j \in \Gamma_\mathrm{S}$ can be obtained using Eqs. (11) and (12) as

$$\begin{aligned} u^{(k+1)}(\boldsymbol{y}_j) &= \sum_{i=1}^{N} \Phi_i(\boldsymbol{y}_j)\hat{u}_i^{(k+1)}, \\ q^{(k+1)}(\boldsymbol{y}_j) &= \sum_{i=1}^{N} \Phi_i(\boldsymbol{y}_j)\hat{q}_i^{(k+1)}. \end{aligned} \tag{23}$$

At each iteration, equation (22) needs to be solved. In the iterative algorithm, the coefficient matrices $\boldsymbol{H}$ and $\boldsymbol{G}$ and the vector $\bar{\boldsymbol{B}}$ only have to be computed at the initial stage. Besides, the MLS shape functions $\Phi_i(\boldsymbol{y}_j)$ used in Eqs. (16), (17), (21), and (23) can also be computed only once, then the matrices $\boldsymbol{M}_1$, $\boldsymbol{M}_2$, and $\boldsymbol{M}_3$ at each iteration can be assembled easily.

The detailed algorithm of the current meshless method for the Signorini problem (1)–(4) can be presented as follows.

1) Choose a tolerance $\tau > 0$ and set $k = 0$.

2) Select N nodes on boundary Γ and compute the shape functions.

3) Assume initially that the boundary condition on the Signorini boundary Γ_S is

$$u^{(0)}(\boldsymbol{x}) = \bar{u}(\boldsymbol{x}), \qquad \boldsymbol{x} \in \Gamma_\mathrm{S}, \tag{24}$$

then equations (1)–(3) and (24) are solved together to obtain $q^{(0)}$ on Γ_S, and we obtain the matrices $\boldsymbol{H}$ and $\boldsymbol{G}$ and the vector $\bar{\boldsymbol{B}}$.

4) Determine Γ_SD and Γ_SR by checking the boundary conditions on Γ_S, then form the boundary value problem (9).

5) Assemble the linear system (22).

6) Solve Eq. (22) to obtain $\hat{\boldsymbol{U}}$ and $\hat{\boldsymbol{Q}}$.

7) Solve Eq. (23) to obtain $u^{(k+1)}(\boldsymbol{y}_j)$ and $q^{(k+1)}(\boldsymbol{y}_j)$ for all nodes $\boldsymbol{y}_j \in \Gamma_\mathrm{S}$.

8) Compute the relative error

$$e(u) = \sqrt{\sum_{\boldsymbol{y}_j \in \Gamma_\mathrm{S}} \left(u^{(k+1)}(\boldsymbol{y}_j) - u^{(k+1)}(\boldsymbol{y}_j)\right)^2 \Big/ \sum_{\boldsymbol{y}_j \in \Gamma_\mathrm{S}} \left(u^{(k+1)}(\boldsymbol{y}_j)\right)^2}.$$

9) If $e(u) > \tau$, update k to $k+1$, and go to step 4). Otherwise, stop the algorithm and return $\hat{\boldsymbol{U}}$ and $\hat{\boldsymbol{Q}}$.

Once the algorithm is terminated, the yet unknown u on $\Gamma_\mathrm{N} \cup \Gamma_\mathrm{S}$ and q on $\Gamma_\mathrm{D} \cup \Gamma_\mathrm{S}$ can be computed using Eqs. (11) and (12), respectively. Then, the numerical solution u of the Signorini problem (1)–(4) at any point inside domain Ω can be computed as

$$\begin{aligned} u(\boldsymbol{y}) = &\sum_{I=1}^{N_\Gamma} \int_{\Gamma_I} u^*(\boldsymbol{x},\boldsymbol{y}) q(\boldsymbol{x})\,\mathrm{d}\Gamma - \sum_{I=1}^{N_\Gamma} \int_{\Gamma_I} q^*(\boldsymbol{x},\boldsymbol{y}) u(\boldsymbol{x})\,\mathrm{d}\Gamma \\ &- \sum_{e=1}^{N_e} \left[\sum_{I=1}^{N_I} w_I (u^* b)_I\right] A_e, \qquad \boldsymbol{y} \in \Omega. \end{aligned} \tag{25}$$

The integrands in Eq. (25) are always regular and can be evaluated by the usual Gaussian quadrature. The integrands in Eq. (14) consist of regular and singular functions. The regular integrals can be computed in the same manner as above, while the singular integrals are handled by the logarithmic Gaussian quadrature and the Cauchy principle value integral formula.[33]

5. Convergence study

In this section, we will prove that the current meshless algorithm generates a sequence of strongly convergent approximations.

Theorem 1 The approximate solution $\left(u^{(k)}, q^{(k)}\right)$ obtained from our algorithm converges to the unique solution (u, q) of the Signorini problem (1)–(4).

Proof According to Eq. (6), we can verify

$$\left\langle u^{(k+1)} - u^{(k)} + c\left(q^{(k+1)} - \bar{q}\right), u^{(k+1)} - u\right\rangle_{\Gamma_\mathrm{S}} \le 0,$$

where the duality $\langle\cdot,\cdot\rangle_{\Gamma_\mathrm{S}}$ is defined for functions w and v as $\langle w, v\rangle_{\Gamma_\mathrm{S}} = \int_{\Gamma_\mathrm{S}} wv\,\mathrm{d}\Gamma$. Thus,

$$\begin{aligned} \left\|u^{(k+1)} - u\right\|_{\Gamma_\mathrm{S}}^2 &= \left\|u^{(k+1)} - \left(u^{(k)} - c\left(q^{(k+1)} - \bar{q}\right)\right)\right. \\ &\quad \left. + \left(u^{(k)} - c\left(q^{(k+1)} - \bar{q}\right)\right) - u\right\|_{\Gamma_\mathrm{S}}^2 \\ &= \left\|\left(u^{(k)} - c\left(q^{(k+1)} - \bar{q}\right)\right) - u\right\|_{\Gamma_\mathrm{S}}^2 \\ &\quad - \left\|u^{(k+1)} - \left(u^{(k)} - c\left(q^{(k+1)} - \bar{q}\right)\right)\right\|_{\Gamma_\mathrm{S}}^2 \\ &\quad + 2\left\langle u^{(k+1)} - u^{(k)} + c\left(q^{(k+1)} - \bar{q}\right), u^{(k+1)} - u\right\rangle_{\Gamma_\mathrm{S}} \\ &\le \left\|u^{(k)} - u - c\left(q^{(k+1)} - \bar{q}\right)\right\|_{\Gamma_\mathrm{S}}^2 \\ &\quad - \left\|u^{(k+1)} - u^{(k)} + c\left(q^{(k+1)} - \bar{q}\right)\right\|_{\Gamma_\mathrm{S}}^2 \\ &= \left\|u^{(k)} - u\right\|_{\Gamma_\mathrm{C}}^2 - \left\|u^{(k+1)} - u^{(k)}\right\|_{\Gamma_\mathrm{S}}^2 \\ &\quad - 2c\left(\left\langle q^{(k+1)} - \bar{q}, u^{(k)} - u\right\rangle_{\Gamma_\mathrm{S}}\right. \\ &\quad \left. - \left\langle q^{(k+1)} - \bar{q}, u^{(k)} - u^{(k+1)}\right\rangle_{\Gamma_\mathrm{S}}\right), \end{aligned} \tag{26}$$

where the norm $\|\cdot\|_{\Gamma_\mathrm{S}}$ is defined for function v as $\|v\|_{\Gamma_\mathrm{S}} = \sqrt{\langle v, v\rangle_{\Gamma_\mathrm{S}}}$.

On the other hand, applying Green's formula leads to

$$\begin{aligned}&\left\langle q^{(k+1)}-\bar{q},u^{(k+1)}-u\right\rangle_{\Gamma_S}-\left\langle q-\bar{q},u^{(k+1)}-u\right\rangle_{\Gamma_S}\\&=\left\langle q^{(k+1)}-q,u^{(k+1)}-u\right\rangle_{\Gamma_S}\\&=\left\|\nabla\left(u^{(k+1)}-u\right)\right\|^2_{L^2(\Omega)}\geq 0.\end{aligned}$$

Then from Eqs. (4) and (6), we have

$$\begin{aligned}&\left\langle q^{(k+1)}-\bar{q},u^{(k+1)}-u\right\rangle_{\Gamma_S}\\&\geq\left\langle q-\bar{q},u^{(k+1)}-u\right\rangle_{\Gamma_S}\\&=\left\langle q-\bar{q},u^{(k+1)}-\bar{u}\right\rangle_{\Gamma_S}-\langle q-\bar{q},u-\bar{u}\rangle_{\Gamma_S}\\&=\left\langle q-\bar{q},u^{(k+1)}-\bar{u}\right\rangle_{\Gamma_S}\geq 0.\end{aligned}$$

Hence,

$$\begin{aligned}&\left\langle q^{(k+1)}-\bar{q},u^{(k)}-u\right\rangle_{\Gamma_S}\\&=\left\langle q^{(k+1)}-\bar{q},u^{(k)}-u^{(k+1)}\right\rangle_{\Gamma_S}+\left\langle q^{(k+1)}-\bar{q},u^{(k+1)}-u\right\rangle_{\Gamma_S}\\&\geq\left\langle q^{(k+1)}-\bar{q},u^{(k)}-u^{(k+1)}\right\rangle_{\Gamma_S}.\end{aligned}\tag{27}$$

Inserting Eq. (26) into Eq. (25) yields

$$\left\|u^{(k+1)}-u\right\|^2_{\Gamma_S}\leq\left\|u^{(k)}-u\right\|^2_{\Gamma_S}-\left\|u^{(k+1)}-u^{(k)}\right\|^2_{\Gamma_S}.\tag{28}$$

Hence, the sequence $\{u^{(k)}\}$ is bounded and

$$\begin{aligned}\sum_{k=0}^{\infty}\left\|u^{(k+1)}-u^{(k)}\right\|^2_{\Gamma_S}&\leq\sum_{k=0}^{\infty}\left(\left\|u^{(k)}-u\right\|^2_{\Gamma_S}-\left\|u^{(k+1)}-u\right\|^2_{\Gamma_S}\right)\\&\leq\left\|u^{(0)}-u\right\|^2_{\Gamma_S}.\end{aligned}$$

Consequently, $\{u^{(k)}\}$ is a Cauchy sequence.

Let (u,q) be a cluster point of the sequence $\{(u^{(k)},q^{(k)})\}$, and the subsequence $\{(u^{(k_1)},q^{(k_1)})\}$ of $\{(u^{(k)},q^{(k)})\}$ converges to (u,q), then (u,q) satisfies Eq. (5). Therefore, from the equivalence of Eqs. (4) and (5), we conclude that (u,q) is the solution of the Signorini problem (1)–(4).

To prove that (u,q) is the unique cluster point of $\{(u^{(k)},q^{(k)})\}$, we assume that $(\tilde{u},\tilde{q})$ is another cluster point and let

$$\delta=\|\tilde{u}-u\|_{\Gamma_S}.$$

Since (u,q) is the cluster point, there exists a positive integer $\bar{k}$ such that $\|u^{(\bar{k})}-u\|_{\Gamma_S}\leq\delta/2$. Besides, equation (28) indicates $\|u^{(k+1)}-u\|_{\Gamma_S}\leq\|u^{(k)}-u\|_{\Gamma_S}$. Then, for any $k>\bar{k}$, we have

$$\left\|u^{(k)}-u\right\|_{\Gamma_S}\leq\frac{\delta}{2}.$$

Hence, according to the triangle inequality,

$$\left\|u^{(k)}-\tilde{u}\right\|_{\Gamma_S}\geq\|\tilde{u}-u\|_{\Gamma_S}-\left\|u^{(k)}-u\right\|_{\Gamma_S}\geq\frac{\delta}{2},$$

which indicates that $\lim_{k\to\infty}u^{(k)}\neq\tilde{u}$. Consequently, the sequence $\{(u^{(k)},q^{(k)})\}$ has only one cluster point (u,q), thus

$$\lim_{k\to\infty}\left(u^{(k)},q^{(k)}\right)=(u,q),$$

which completes the proof.

6. Numerical examples

In this section, the current meshless algorithm is applied to study several Signorini problems, and the results are compared with those obtained by the BEM to verify the accuracy and the advantage of the new meshless algorithm. In this paper, all numerical codes are implemented in MATLAB 7.0.1, and the computations have been carried out on a desktop PC with an Intel 2.93 GHz CPU and 2 GB of RAM.

6.1. Signorini problem for the Poisson equation

Consider the following Signorini problem:

$$\begin{aligned}&\Delta u(x_1,x_2)=-\cos\left(\frac{\pi}{2}+\pi x_1\right)-1,\\&(x_1,x_2)\in\Omega=(0,1)\times(0,1),\end{aligned}$$

with the Dirichlet and the Neumann boundary conditions

$$\begin{aligned}&u(0,x_2)=0,\ \ u(1,x_2)=0,\quad 0\leq x_2\leq 1,\\&q(x_1,1)=-7x_1(1-x_1),\qquad 0\leq x_1\leq 1,\end{aligned}$$

and the Signorini boundary conditions

$$\begin{aligned}&u\leq\bar{u},\ \ q\leq 0,\ \ (u-\bar{u})q=0,\\&(x_1,x_2)\in\Gamma_S=\{(x_1,x_2):0\leq x_1\leq 1,x_2=0\},\end{aligned}$$

where $\bar{u}(x_1,x_2)=5x_1(1-x_1)(0.5-x_1)\max(x_1,1-x_1)$.

The numerical results for u on Γ_S are plotted in Fig. 1. The results for q are plotted in Fig. 2. In this analysis, 32 boundary nodes are used to discretize per side of the domain. These results are compared with the solutions of the BEM.[11] Although no analytical solutions exist for this problem, it is evident that the solutions of the presented algorithm are in good agreement with the results of the BEM.

For the purpose of error estimation and convergence studies, the problem is solved by choosing different numbers of boundary nodes. The error

$$e(v)=\sqrt{\sum_{\boldsymbol{y}_j\in\Gamma_S}\left(v(\boldsymbol{y}_j)-v_h(\boldsymbol{y}_j)\right)^2\Big/\sum_{\boldsymbol{y}_j\in\Gamma_S}\left(v(\boldsymbol{y}_j)\right)^2}$$

is defined to evaluate the method performance, where v and v_h are analytical and numerical solutions, respectively.

Since the analytical solution of the problem is not known, the error is estimated by substituting the analytical solutions with some selected approximate ones which can be computed with more boundary nodes. In this work, we obtain these approximate solutions by using our algorithm with 3000 boundary nodes. Figures 3 and 4 show the log–log plot of the errors obtained by our algorithm and the BEM.[11] The results show that the more nodes there are, the greater precision we obtain.

With the same number of nodes, our algorithm has smaller errors than the BEM. So to obtain the same precision, our algorithm needs fewer nodes. The results show that our algorithm has a better convergence characteristic.

The corresponding CPU time is shown in Table 1, from which we can see that the CPU time of our algorithm is less than that of the BEM. Thus, our algorithm has not only a higher convergence rate but also a greater computational precision and a better efficiency than the BEM.

Table 1. CPU time (in seconds) of our algorithm and the BEM.

Number of nodes	32	64	128	256	512	1024
BEM	0.109	0.187	0.515	1.781	8.218	47.297
Our algorithm	0.093	0.140	0.266	0.781	3.938	24.812

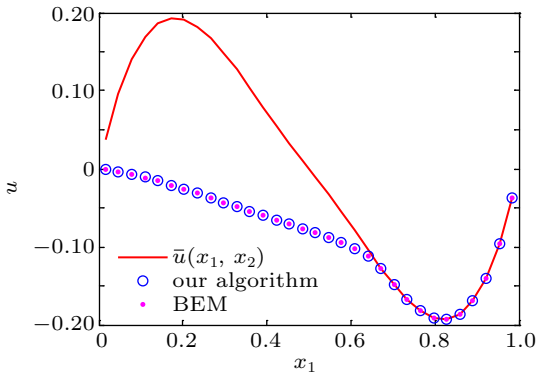


Fig. 1. (color online) Numerical results for u on Γ_S.

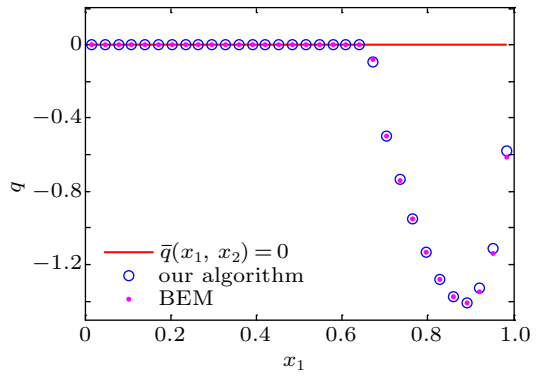


Fig. 2. (color online) Numerical results for q on Γ_S.

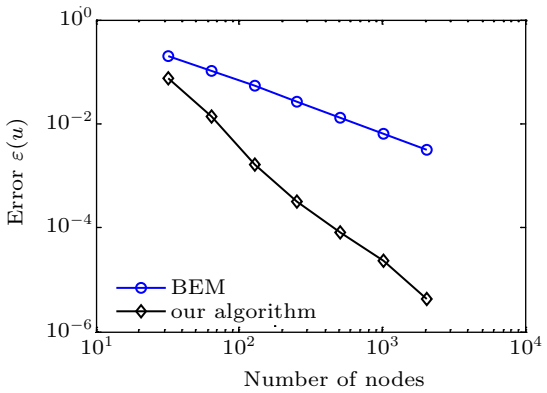


Fig. 3. (color online) Convergence of u.

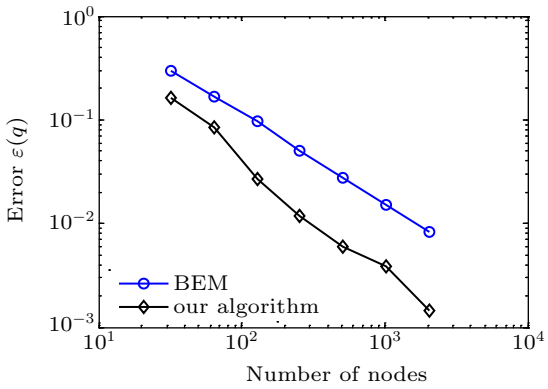


Fig. 4. (color online) Convergence of q.

6.2. The electropainting problem

The electropainting problem describes the coating process of a metal surface with paint.[4] This problem can be formulated as a Signorini problem for the electric potential. In the paint solution, the electric potential u satisfies

$$\Delta u(x_1,x_2) = 0, \qquad (x_1,x_2) \in \Omega = (0,0.5) \times (0,1),$$

with the Dirichlet and the Neumann boundary conditions

$$u(x_1,0) = 1, \qquad 0 \le x_1 \le 0.5,$$
$$q(0,x_2) = 0, \qquad 0 \le x_2 \le 1,$$

and the Signorini boundary conditions

$$u \ge 0, \;\; q+\gamma \ge 0, \;\; u(q+\gamma) = 0, \qquad (x_1,x_2) \in \Gamma_S,$$

where the known constant γ is the critical cut-off current and is a property of the paint, and the Signorini boundary

$$\Gamma_S = \{(x_1,x_2) : x_1 = 0.5, 0 \le x_2 \le 1\}$$
$$\cup \{(x_1,x_2) : 0 \le x_1 \le 0.5, x_2 = 1\}$$

makes up the workpiece to be painted. On Γ_S, we have to decide which parts need to be painted ($u > 0, q+\gamma = 0$) and which parts do not need to be painted ($u = 0, q+\gamma > 0$).

For various values of γ, the numerical results for u on the Signorini boundary Γ_S are presented in Figs. 5–8. In this analysis, we employ 30 nodes on the boundary. The results are compared with the solutions of the BEM.[10] Note that the results are shown as plots over the arc-length s, $s = 0$ corresponds to the origin $O(0,0)$ and counter-clockwise parametrization of the boundary Γ. Clearly, $s = 0.5$, $s = 1.5$, and $s = 2$ correspond to the vertexes $(0,0.5)$, $(0.5,1)$, and $(0,1)$, respectively. From these figures, it can be seen again that the present results are in excellent agreement with those of the BEM.

In Fig. 9, we plot the paint distributions over the domain obtained for various values of γ. In this analysis, we use 240 nodes on the boundary. For a small γ, the workpiece is completely painted with the corner receiving the least amount of paint, as shown in Fig. 9(a). If γ is increased, the paint film near the corner becomes thinner (Fig. 9(b)) and eventually unpainted (Fig. 9(c)). With a higher γ, both the corner and the top boundary are unpainted (Fig. 9(d)). Therefore, although there

are no analytical solutions available to verify the results of the current meshless algorithm for such a complex problem, the reliability can be judged from the reasonable physical characteristics. Besides, the present results are in good agreement with those given in Refs. [4], [8], and [10].

To investigate the convergence, we compare the relative errors with different values of γ. The error is estimated by substituting the exact solutions with approximate ones obtained using 3000 boundary nodes. The relationship between the error and the number of nodes is given in Fig. 10, which shows that the solution converges as the number of nodes increases. Besides, we can observe that the experimental convergence rate is very high and approximates to 2.

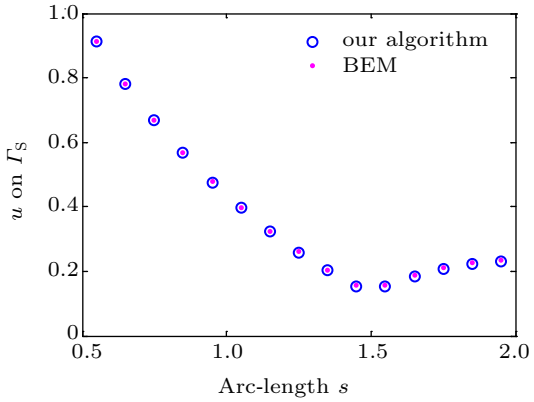


Fig. 5. (color online) Numerical results of the electropainting problem for $\gamma = 0.4$.

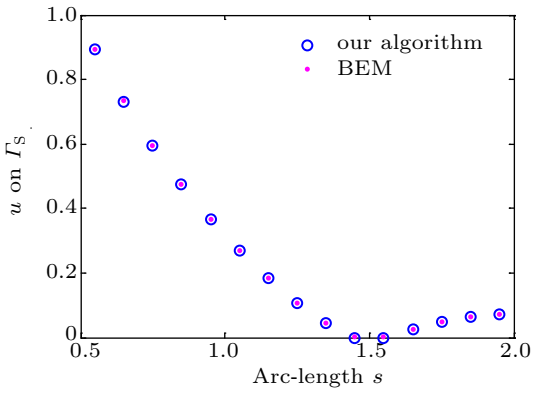


Fig. 6. (color online) Numerical results of the electropainting problem for $\gamma = 0.5$.

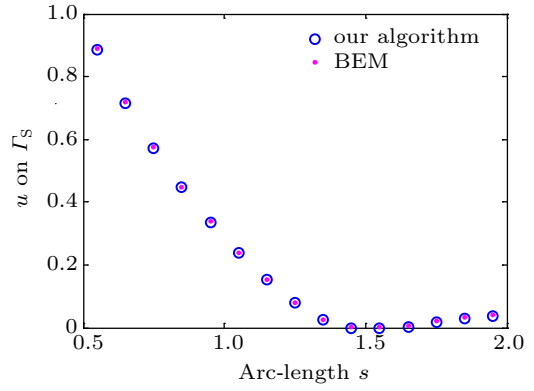


Fig. 7. (color online) Numerical results of the electropainting problem for $\gamma = 0.55$.

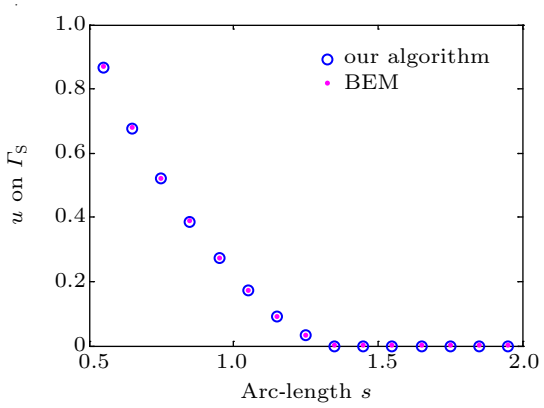


Fig. 8. (color online) Numerical results of the electropainting problem for $\gamma = 0.7$.

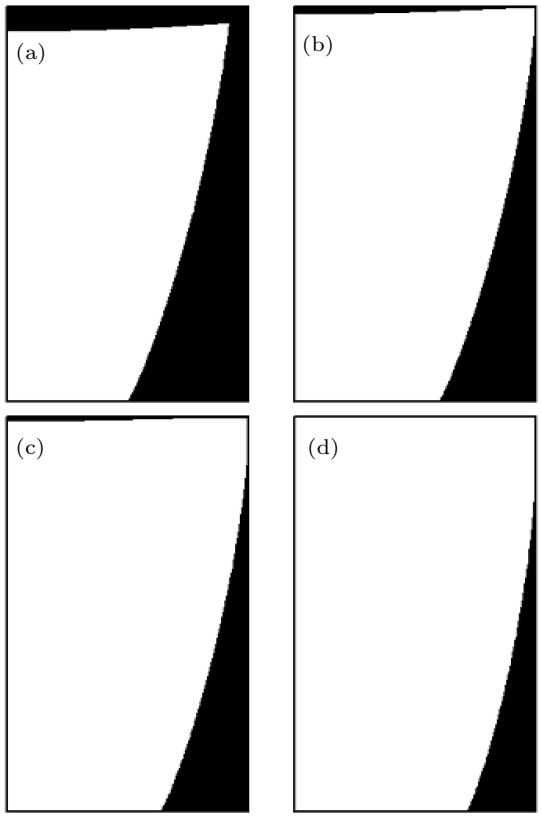


Fig. 9. Paint distributions for (a) $\gamma = 0.4$, (b) $\gamma = 0.5$, (c) $\gamma = 0.55$, and (d) $\gamma = 0.7$.

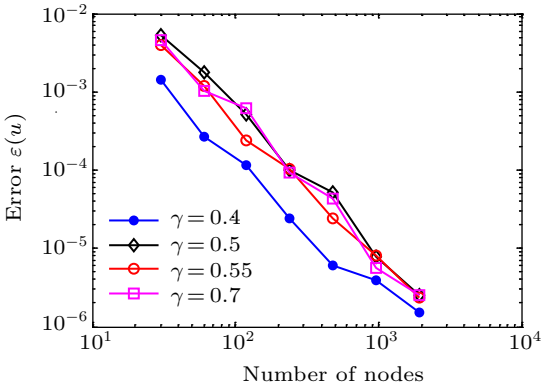


Fig. 10. (color online) Convergence in the electropainting problem.

6.3. Problem on a half-torus domain

The example is a Signorini problem on a half-torus domain. The analytical solution is given by the following complex function:[9]

$$u(\boldsymbol{x}) = \mathrm{Im}\left(\sqrt{A+B}\mathrm{sign}x_1 + \mathrm{i}\sqrt{A-B}\mathrm{sign}x_2\right)^3$$
$$\text{in } \Omega = \{\boldsymbol{x} = (x_1, x_2) : a < |\boldsymbol{x}| < b, x_2 \le 0\},$$

where

$$A = \frac{1}{2}\sqrt{\left(\frac{x_1^2 - x_2^2}{|\boldsymbol{x}|^2}\right)^2 + \frac{1}{4}\left(\frac{|\boldsymbol{x}|^2 - a^2}{a^2|\boldsymbol{x}|^2}\right)^2}$$

and

$$B = \frac{\left(x_1^2 - x_2^2\right)\left(|\boldsymbol{x}|^2 + a^2\right)}{4a^2|\boldsymbol{x}|^4},$$

with $|\boldsymbol{x}| = \sqrt{x_1^2 + x_2^2}$. The Dirichlet boundary conditions corresponding to the analytical solution are given on the noncontact boundary $\Gamma_{\mathrm{D}} = \{\boldsymbol{x} : |\boldsymbol{x}| = b, x_2 < 0\} \cup \{\boldsymbol{x} : a < |\boldsymbol{x}| < b, x_2 = 0\}$. The Signorini boundary conditions on the contact boundary $\Gamma_{\mathrm{S}} = \{\boldsymbol{x} : |\boldsymbol{x}| = a, x_2 < 0\}$ are $u \ge 0$, $q \ge 0$, and $uq = 0$.

In the numerical calculations, we take $a = 0.1$ and $b = 0.25$, and use the parameterization $t \to (a\cos 2\pi t, -a\sin 2\pi t)$. The results for u and q on Γ_{S} are plotted in Figs. 11 and 12, respectively. In this analysis, we use 140 boundary nodes. It is evident that the numerical results of our algorithm agree well with the analytical ones.

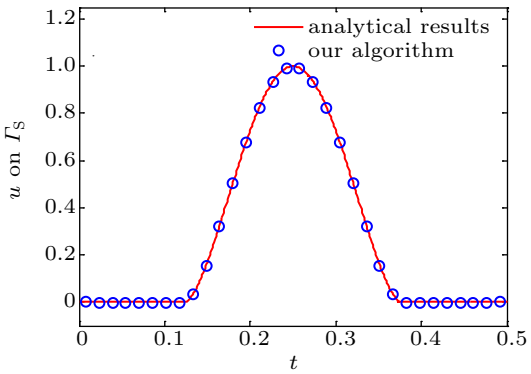


Fig. 11. (color online) Analytical and numerical solutions for u on Γ_{S}.

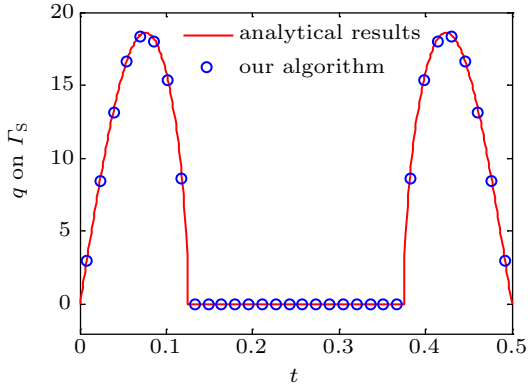


Fig. 12. (color online) Analytical and numerical solutions for q on Γ_{S}.

7. Conclusion

Based on the MLS approximation, a meshless algorithm has been presented for elliptic Signorini problems. The algorithm requires only a nodal data structure on the boundary of the domain to be solved. Besides, nonlinear boundary inequality constraints are incorporated into the iterative scheme and thus can be applied with ease. Moreover, since the Signorini boundary is of prime interest, this algorithm is particularly suitable for Signorini problems. The theoretical convergence study shows that the algorithm can generate a sequence of strongly convergent approximations. Some examples have been given and the numerical results are in excellent agreement with the previously reported numerical solutions. We have shown that this algorithm has not only a better convergence characteristic but also a greater computational efficiency than the BEM. In conclusion, the proposed algorithm is very effective in solving Signorini problems.

References

[1] Signorini A 1993 *Annali della Scuola Normale superiore di Pisa, Classe di Scienze* **2** 231
[2] Fichera G 1964 *Mem. Accad. Naz. Lincei.* **5** 91
[3] Aitchison J M, Elliott C M and Ockendon J R 1983 *IMA J. Appl. Math.* **30** 269
[4] Aitchison J M, Lacey A A and Shillor M 1984 *IMA J. Appl. Math.* **33** 17
[5] Howison D, Morgan J D and Ockendon J R 1997 *SIAM Rev.* **39** 221
[6] Ito K and Kunisch K 2008 *Appl. Math.* **53** 445
[7] Aitchison J M and Poole M W 1998 *J. Comput. Appl. Math.* **94** 55
[8] Poullikkas A, Karageorghis A and Georgiou G 1998 *IMA J. Numer. Anal.* **18** 273
[9] Spann W 1993 *Numer. Math.* **65** 337
[10] Zhang S G and Zhu J L 2012 *Eng. Anal. Bound. Elem.* **36** 112
[11] Zhang S G and Zhu J L 2013 *Eng. Anal. Bound. Elem.* **37** 176
[12] Lancaster P and Salkauskas K 1981 *Math. Comput.* **37** 141
[13] Cheng Y M and Chen M J 2003 *Acta Mech. Sin.* **35** 181 (in Chinese)
[14] Wang J F, Sun F X and Cheng Y M 2012 *Chin. Phys. B* **21** 090204
[15] Sun F X, Wang J F and Cheng Y M 2013 *Chin. Phys. B* **22** 120203
[16] Wang J F and Cheng Y M 2013 *Chin. Phys. B* **22** 030208
[17] Wang Q F, Dai B D and Li Z F 2013 *Chin. Phys. B* **22** 080203
[18] Shi T Y, Cheng R J and Ge H X 2013 *Chin. Phys. B* **22** 060210
[19] Wang F, Lin G, Zheng B J and Hu Z Q 2013 *Chin. Phys. B* **22** 060206
[20] Li Q H, Chen S S and Zeng J H 2013 *Chin. Phys. B* **22** 120204
[21] Li S L and Li X L 2014 *Chin. Phys. B* **23** 028702
[22] Mukherjee Y X and Mukherjee S 1997 *Int. J. Numer. Methods Eng.* **40** 797
[23] Miao Y, He T, Yang Q and Zheng J 2010 *Eng. Anal. Bound. Elem.* **34** 755
[24] Wang Q, Miao Y and Zhu H 2013 *Comput. Mech.* **51** 885
[25] Miao Y, Li W, Lv J and Zhu H 2013 *Eng. Anal. Bound. Elem.* **37** 1311
[26] Cheng Y M and Peng M J 2005 *Sci. China: Phys. Mech. Astron.* **48** 641
[27] Ren H P, Cheng Y M and Zhang W 2010 *Sci. China: Phys. Mech. Astron.* **53** 758
[28] Wang J F, Sun F X and Cheng Y M 2013 *Int. J. Comput. Methods* **10** 6
[29] Li X L and Zhu J L 2009 *J. Comput. Appl. Math.* **230** 314
[30] Li X L 2011 *Appl. Numer. Math.* **61** 1237
[31] Li X L and Li S L 2013 *Chin. Phys. B* **22** 080204
[32] Noor M A 2010 *J. Appl. Math. Comput.* **32** 83
[33] Zhu J L and Yuan Z Q 2009 *Boundary Element Analysis* (Beijing: Science Press) (in Chinese)